water

MDPI

Article

Physics-Guided Deep Learning for Spatiotemporal Evolution of Urban Pluvial Flooding

Hyuna Woo, Hyeonjin Choi, Minyoung Kim and Seong Jin Noh *

Department of Civil Engineering, Kumoh National Institute of Technology, Gumi 39177, Republic of Korea; hwoo@kumoh.ac.kr (H.W.); hyeonjin21@kumoh.ac.kr (H.C.); minyy208@kumoh.ac.kr (M.K.)
* Correspondence: seongjin.noh@kumoh.ac.kr

Abstract: Climate change and rapid urbanization have increased the risk of urban flooding, making timely and accurate flood prediction crucial for disaster response. However, conventional physics-based models are limited in real-time applications due to their high computational costs. Recent advances in deep learning have enabled the development of efficient surrogate models that capture complex nonlinear relationships in hydrological processes. This study presents a deep learning-based surrogate model designed to efficiently reproduce the spatiotemporal evolution of urban pluvial flooding using data from physics-based models. For the Oncheon-cheon catchment in Busan, the spatiotemporal evolution of inundation at a 10 m spatial resolution was simulated using the physics-based model for various synthetic inundation scenarios to train the deep learning model based on a Convolutional Neural Network (CNN). The training dataset was constructed using synthetic rainfall scenarios based on probabilistic rainfall data, while the model was validated using both a synthetic flood event and a historical flood event from July 2020 with observed ground-based rainfall measurements. The model's performance was evaluated using quantitative metrics, including the Hit Rate (HR), False Alarm Ratio (FAR), and Critical Success Index (CSI), by comparing results against both synthetic and real (historical) flood events. Validation results demonstrated high reproducibility, with a CSI of 0.79 and 0.73 for the synthetic and real experiments, respectively. In terms of computational efficiency, the deep learning model achieved a speedup 16.4 times the parallel version and 82.2 times the sequential version of the physics-based model, demonstrating its applicability for near real-time flood prediction. The findings of this study contribute to the advancement of urban flood prediction and early warning systems by offering a cost-effective, computationally efficient alternative to conventional physics-based flood modeling, enabling faster and more adaptive flood risk management.

Keywords: artificial intelligence; deep learning; physics-guided; urban pluvial flooding

check for updates

Academic Editor: Olga Petrucci

Received: 10 March 2025
Revised: 11 April 2025
Accepted: 16 April 2025
Published: 21 April 2025

Citation: Woo, H.; Choi, H.; Kim, M.; Noh, S.J. Physics-Guided Deep Learning for Spatiotemporal Evolution of Urban Pluvial Flooding. *Water* **2025**, *17*, 1239. https://doi.org/10.3390/w17081239

1. Introduction

Extreme weather events associated with climate change have become increasingly frequent worldwide, causing significant increases in flood-related damage due to intensified precipitation events [1]. Over the past several decades, global urban exposure to flooding has grown markedly, reflecting the rapid expansion of urban areas into flood-prone zones [2]. This increased vulnerability is especially concerning, as simultaneous urbanization and climate change act as compounding drivers that alter hydrological regimes and amplify surface runoff volumes [3]. Despite these escalating risks, pluvial flooding in urban environments has received comparatively less scholarly attention than other flood types, even though its importance is increasing under changing climatic conditions [4]. Urban flooding is particularly challenging, as it results from the interaction of multiple factors, including rainfall intensity, topography, tidal influences, urban drainage infrastructure, and changes in land use driven by ongoing urban expansion [5]. These combined factors not only increase flood risk but also complicate the accurate prediction and timely forecasting required for effective flood mitigation and emergency response. However, achieving both high accuracy and computational efficiency in urban flood forecasting remains difficult due to the inherent complexity and dynamic nature of urban hydrological processes [6,7].

Physics-based hydrodynamic models, which simulate flood dynamics by solving mathematical equations based on fundamental physical laws governing hydrologic processes, are the traditional tools for urban flood forecasting [8–11]. Widely used models in this category include the Storm Water Management Model (SWMM), Hydrologic Engineering Center's River Analysis System (HEC-RAS), LISFLOOD, and the Modular Integrated Knowledge Engine (MIKE), among many others [8,12–15]. The integration of hydrodynamic models, such as coupling one-dimensional (1D) and two-dimensional (2D) approaches or combining hydrologic and hydraulic models like HEC-HMS with HEC-RAS, has enhanced predictive accuracy for urban flooding by providing more detailed simulations of flood propagation [16–22]. Despite their accuracy, these physics-based approaches—particularly those solving the Shallow Water Equations (SWEs)—require significant computational resources and extensive calibration, which can limit their scalability and real-time applicability. Advances in parallel computing and the use of graphics processing units (GPUs) have partially alleviated these limitations by improving computational efficiency. For example, Noh et al. [23] developed a hybrid code for efficient urban flood modeling, and Morales-Hernández et al. [24] proposed a GPU-accelerated 2D hydrodynamic model. Similarly, Luan et al. [25] implemented a GPU-accelerated coupled 1D-2D flood model for high-resolution simulations of urban hydrology. Simplified approaches, such as Cellular Automata (CA), have also been proposed to reduce computational costs by routing surface runoff using simplified rules based on water depth and terrain roughness rather than directly solving complex physical equations [26–29]. Beyond optimizing computational performance in physics-based modeling, data-driven approaches have emerged as viable alternatives. Some studies have explored the use of citizen-contributed data for flood monitoring, extracting water level information from social media and crowdsourced observations [30–33]. While such real-time, observation-based methods offer valuable insights for enhancing flood situational awareness, their forecasting capability remains limited due to data sparsity and inconsistency.

Recent advances in deep learning have introduced new possibilities in hydrological modeling, with deep learning-based methods emerging as effective alternatives for predicting flood inundation extent and depth [34–37]. Unlike physics-based models, deep learning models identify complex nonlinear relationships directly from data without explicitly modeling physical interactions between hydrological variables, offering significant computational advantages once trained [38]. Various deep learning architectures have been applied to urban flood prediction, including Artificial Neural Networks (ANNs), CNNs, Long Short-Term Memory (LSTM) networks, and Generative Adversarial Networks (GANs) [39–44]. These data-driven methods have become particularly valuable for real-time flood forecasting, leveraging historical event data to support timely risk assessment and response [45].

Several studies have explored the use of deep learning-based flood models. Löwe et al. [46] introduced U-FLOOD, a U-Net-based model for predicting inundation maps using terrain data. Hofmann and Schüttrumpf [47] developed FloodGAN, a model that transforms rainfall data into spatial flood extent predictions. Additionally, hybrid approaches incorporating encoder–decoder networks, Graph Neural Networks (GNNs), and GANs have demonstrated effectiveness in capturing complex spatiotemporal flood patterns [48].

Despite these advances, fully data-driven deep learning models face key limitations, including their high dependence on large volumes of training data and their tendency to overlook detailed spatiotemporal flood dynamics. As a result, their interpretability and adaptability to diverse urban conditions remain limited [47,49]. To address these challenges, researchers have increasingly focused on integrating deep learning with physical modeling principles, a concept often referred to as physics-informed machine learning [50]. By incorporating physically based constraints and hydrodynamic knowledge into deep learning models, hybrid approaches have demonstrated potential for improving predictive accuracy, enhancing model robustness, and increasing transferability across different flood scenarios [1,5,51,52].

Hybrid physics-guided approaches mitigate the shortcomings of purely data-driven deep learning models, which often lack sufficient real-world flood data, particularly for rare extreme events. By leveraging physics-based hydrodynamic models as training data, these hybrid methods enable deep learning models to learn realistic flood dynamics while maintaining computational efficiency. This integration enhances prediction reliability and physical consistency, making deep learning models more applicable to urban flood modeling, where stormwater drainage interactions, surface flow complexities, and built-environment factors significantly influence flood dynamics.

This study proposes a physics-guided CNN model designed to simulate the spatiotemporal dynamics of pluvial flooding in urban areas. The inundation database used for training and validating the model is generated using physics-based hydrodynamic simulations, encompassing diverse synthetic flooding scenarios. The predictive performance of the proposed CNN model is evaluated using both synthetic and historical rainfall events for the Oncheon-cheon catchment in Busan. We quantitatively assess key parameters such as spatiotemporal flood progression, inundation depth distribution, and flow characteristics by comparing CNN outputs with benchmark hydrodynamic simulations. Furthermore, we evaluate the computational efficiency of the proposed CNN model, demonstrating substantial reductions in computational time compared with traditional physics-based hydrodynamic models, thus highlighting its potential applicability in real-time urban flood forecasting and emergency response operations.

2. Materials and Methods

2.1. Framework of Deep Learning-Based Urban Flood Predictions

The proposed framework for urban flood prediction, depicted in Figure 1, consists of two primary phases: preprocessing and deep learning model development. In the data preprocessing phase, synthetic rainfall scenarios are initially generated to represent diverse rainfall intensities and durations, covering a wide range of potential flooding conditions. These synthetic rainfall inputs are simulated using a physics-based hydrodynamic model, producing a comprehensive database of corresponding flood scenarios. This inundation database is then divided into training and test datasets, with the training dataset composed exclusively of synthetic rainfall events and their flood outcomes. The test dataset, on the other hand, comprises historical rainfall events with their observed flooding conditions, enabling the assessment of model performance under realistic conditions. In the deep learning modeling phase, a CNN is developed and trained using the synthetic dataset to learn and predict flood characteristics. Once trained, the CNN model rapidly predicts flood inundation characteristics, including inundation extent, depth distribution, and temporal flood progression, based on rainfall inputs. Finally, the performance of the CNN is quantitatively evaluated using the test dataset of historical rainfall events, where predicted flood characteristics are compared against those obtained from traditional hydrodynamic simulations. This evaluation considers prediction accuracy and computational efficiency, ensuring the proposed CNN framework is suitable for practical, near real-time urban flood forecasting applications. In this study, the model was trained using 12 synthetic rainfall scenarios, while validation was performed using the real rainfall event of 23 July 2020, with hourly data generated through the Thiessen polygon method. For hyperparameter selection, we manually tested various combinations of kernel sizes, batch sizes, and filter numbers to identify the optimal configuration that maximizes prediction accuracy while maintaining computational efficiency suitable for near real-time applications.

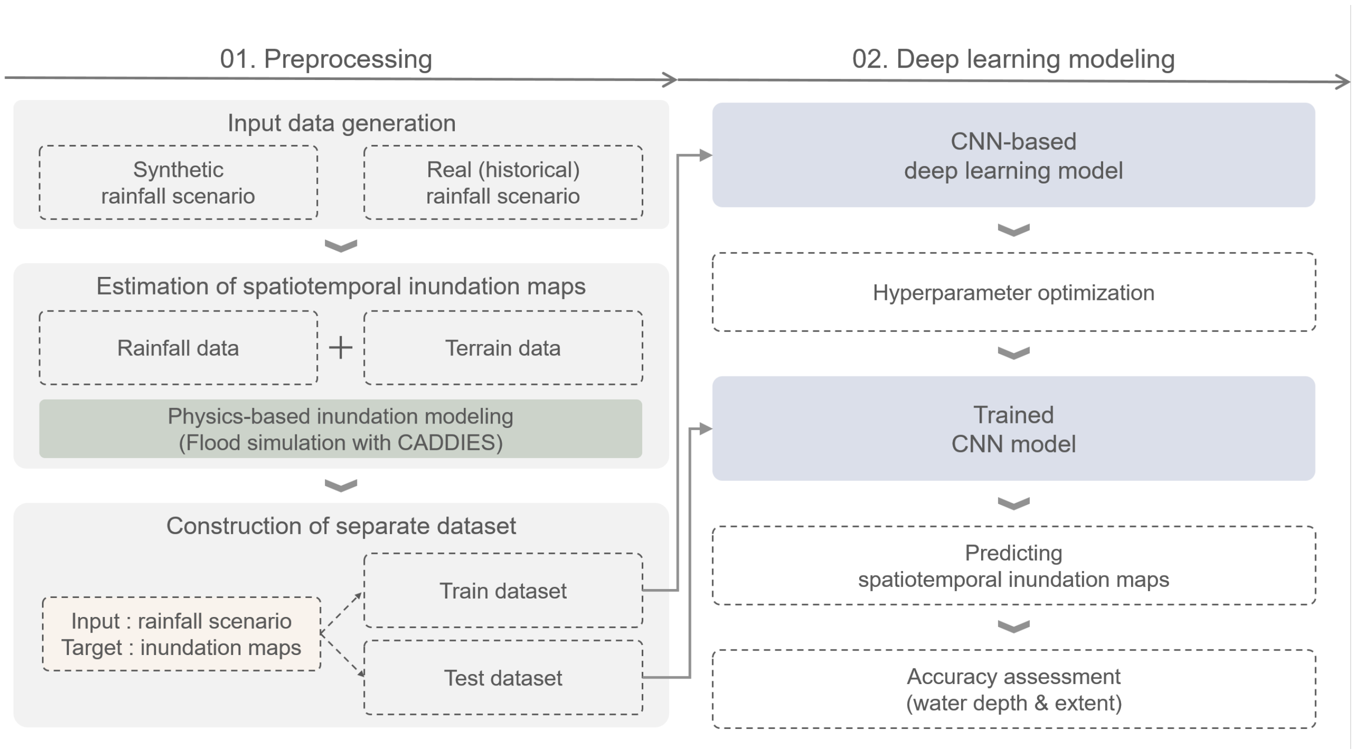

Figure 1. Diagram of deep learning framework for urban flood prediction.

2.2. Physics-Based Inundation Model

In this study, we utilized the CA Dual-DraInagE Simulation (CADDIES)-caflood model (CADDIES-caflood here after), a 2D flood simulation tool based on the CA algorithm, which offers efficient numerical calculations by employing grid-based methodologies for fast computation [27,28]. Within CADDIES-caflood, each grid cell incorporates terrain elevation and surface roughness characteristics, enabling rapid routing of surface runoff using simplified hydrodynamic rules. For this study, we applied a Manning's roughness coefficient of 0.15 for the entire study area, along with a runoff coefficient of 0.4. These parameter values were adopted from previous work that validated the CADDIES-caflood model for the Oncheon Stream catchment [53]. For a detailed description of the underlying methods, see Guidolin et al. [28]. The CADDIES-caflood model has been validated previously across various urban catchments, demonstrating its reliability in simulating urban inundation processes [53–57]. The model software CADDIES-caflood (version 120) is provided in three variants optimized for different computational resources: (i) a sequential (single-core) version without parallelization, (ii) an OpenMP-based parallel version suitable for multi-core CPUs, and (iii) an OpenCL-based parallel version capable of leveraging GPU acceleration. In the current study, flood simulations were performed using the sequential and OpenMP-based versions of CADDIES-caflood, executed exclusively on CPUs, without considering GPU-based parallel computation.

2.3. Deep Learning-Based Flood Prediction Model (CNN)

The proposed deep learning model used for urban flood prediction is based on a CNN architecture specifically designed to effectively capture and predict the spatiotemporal patterns of urban pluvial flooding from rainfall data. The model architecture, as illustrated in Figure 2, comprises multiple convolutional layers, batch normalization layers, rectified linear unit (ReLU) activation functions, dropout layers, and fully connected layers.

Specifically, the CNN architecture includes two initial convolutional layers, each using 32 filters with a kernel size of 3 to progressively extract spatial and temporal features from the input rainfall data. Both convolutional layers are followed by batch normalization layers to stabilize training and accelerate convergence, and ReLU activation functions to introduce nonlinearity. The extracted features from the convolutional blocks are then passed through fully connected layers to capture deeper feature interactions for accurate flood prediction. The fully connected network consists of three sequential layers with 32, 256, and 512 neurons, respectively. Each fully connected layer is followed by batch normalization, ReLU activation, and dropout layers (with dropout rates of 0.2) to improve generalization and prevent overfitting (Figure 2).

The CNN model's training involves optimizing its parameters over 50 epochs using the synthetic rainfall and inundation datasets. This number of epochs was determined experimentally after evaluating the convergence patterns of the loss function with our limited training dataset, finding that 50 epochs provided an optimal balance between model performance and computational efficiency. During training, the Adam optimizer was applied with the mean squared error (MSE) as the loss function to ensure efficient convergence. The Adam optimizer was selected due to its efficiency in handling sparse gradients and adaptive learning rate capabilities, typically leading to faster and stable convergence in various deep learning applications, including hydrological predictions. For hyperparameter selection, we implemented a manual grid search approach, systematically testing combinations of kernel sizes (1, 3, 5), batch sizes (16, 32, 64), and filter numbers (32, 64, 128) to determine the configuration that optimized prediction accuracy while maintaining computational efficiency for real-time applications. The model architecture and training strategies were selected based on their demonstrated capability to accurately capture complex, nonlinear spatiotemporal patterns associated with urban flooding, thus enabling rapid flood prediction once the model is trained.

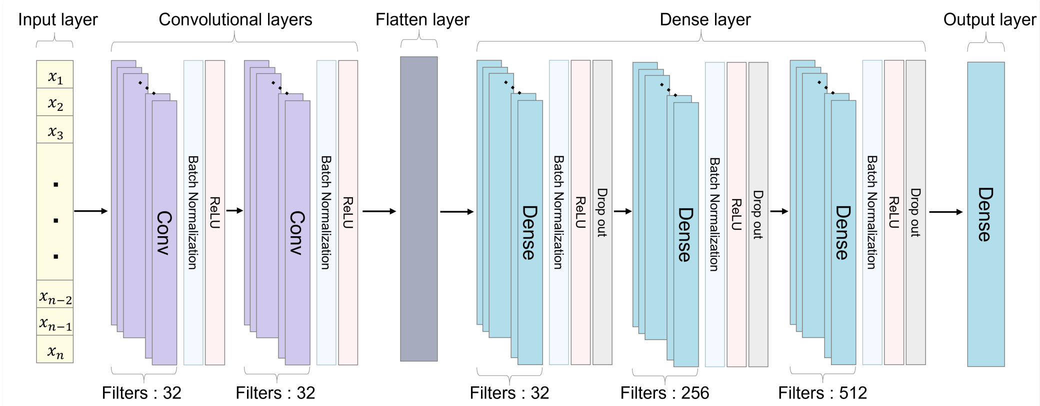

Figure 2. Architecture of CNN model.

2.4. Performance Assessment

2.4.1. Binary Classification Measures

To quantitatively assess flood prediction performance, three binary classification measures—CSI, HR, and FAR—were used. Areas were classified as flooded if inundation depth exceeded 15 cm, and non-flooded otherwise. This threshold aligns with guidelines from the UK Environment Agency, which identifies inundation depths above 15 cm as significantly hazardous [11,58]. Similarly, governmental agencies in South Korea commonly adopt 15 cm as the official threshold for flood warnings, inundation alerts, and emergency responses [59].

In Table 1, *a* represents grids classified as flooded in the CNN model, *b* represents grids classified as flooded in the benchmark CADDIES-caflood model, *c* represents grids classified as non-flooded in the CNN model, and *d* represents grids classified as non-flooded in the CADDIES-caflood model.

Table 1. Grid descriptors in binary classification measures.

	Inundated Grid in CNN	Non-Inundated Grid in CNN
Inundated grid in CADDIES-caflood	*a* (Hits)	*c* (Misses)
Non-inundated grid in CADDIES-caflood	*b* (False alarms)	*d* (True negatives)

(1) HR

The HR represents the flood area ratio of the CNN model relative to the CADDIES-caflood model. The equation is given in Equation (1), which indicates the model's tendency to underestimate flood risk. The HR ranges from 0 to 1, with values closer to 1 indicating better alignment between the CNN model's and CADDIES-caflood model's flood areas.

$$HR = \frac{a}{a+c} \quad (1)$$

(2) FAR

The FAR represents the ratio of areas classified as flooded by the CNN model within non-flooded areas in the CADDIES-caflood model. The equation is given in Equation (2), serving as an indicator of the model's overprediction of flood extent. The range is from 0 to 1, with 0 indicating no false alarms.

$$FAR = \frac{b}{a+b} \quad (2)$$

(3) CSI

The CSI is a comprehensive performance indicator that considers both over- and underprediction, as shown in Equation (3). It ranges from 0 to 1, with 1 indicating perfect alignment between the CNN and CADDIES-caflood model flood areas.

$$CSI = \frac{a}{a+b+c} \quad (3)$$

2.4.2. Flood Depth Prediction Measures

To evaluate the accuracy and reliability of flood depth prediction performance, we employed three assessment metrics: Root Mean Square Error (RMSE), Mean Absolute Error (MAE), and the coefficient of determination (R^2). These metrics provide complementary insights into the model's predictive precision, error magnitude, and ability to replicate the spatial variability of flood depths.

(1) Root Mean Square Error (RMSE)

RMSE is defined as the square root of the arithmetic mean of the squared residuals between predicted and benchmark values. This metric is widely used to evaluate the accuracy of flood depth predictions, emphasizing larger errors and providing a conservative assessment of model performance. The equation is given as:

$$RMSE = \sqrt{\frac{1}{N}\sum_{i=1}^{N}(y_i - \hat{y}_i)^2} \tag{4}$$

where N is the total number of simulation grids, y_i represents the observation or benchmark model (in this case, CADDIES-caflood model's flood depth), and $\hat{y}_i$ represents the simulated result (CNN model's flood depth).

(2) Mean Absolute Error (MAE)

MAE is defined as the arithmetic mean of the absolute differences between predicted and benchmark values. This metric measures the average magnitude of errors without considering their direction, treating all deviations equally regardless of their sign. Unlike RMSE, it is less sensitive to outliers and provides an intuitive measure of the typical prediction error. The equation is given as:

$$MAE = \frac{1}{N}\sum_{i=1}^{N}|y_i - \hat{y}_i| \tag{5}$$

(3) Coefficient of Determination (R^2)

R^2 is defined as the proportion of variance in the benchmark data that is explained by the CNN model. This metric evaluates how well the predicted flood depths capture the variability in the benchmark data, with values ranging from 0 to 1. A value of 1 denotes perfect prediction, while 0 indicates no explanatory power. Negative values suggest performance worse than using the mean as a prediction. The equation is given as:

$$R^2 = 1 - \frac{\sum_{i=1}^{N}(y_i - \hat{y}_i)^2}{\sum_{i=1}^{N}(y_i - \bar{y})^2} \tag{6}$$

where $\bar{y}$ represents the mean of the observation or benchmark model values (CADDIES-caflood model's flood depths).

2.5. Study Area and Data

The study area is the Oncheon-cheon catchment, with an area of 56.3 km^2 and a stream length of 14.1 km, located in Busan, South Korea. Oncheon-cheon, the first tributary of the Suyeong River, flows through a densely urbanized watershed characterized by complex topography. The catchment exhibits steep slopes upstream, ranging approximately from 1/40 to 1/520, and transitions downstream into relatively flat terrain with gentle slopes of about 1/840 to 1/1000. This varied topography, combined with the catchment's extensive urbanization, contributes significantly to its vulnerability to pluvial flooding. Historically, intense rainfall events have frequently caused severe flooding and damage in this area. In particular, the pluvial flooding event in 2020, which is used in this study for model validation, resulted in multiple fatalities and extensive inundation of low-lying urban areas. This susceptibility to recurring flooding emphasizes the critical importance of accurate and timely flood forecasting and effective flood management strategies [59].

For the CADDIES-caflood simulations, a Digital Surface Model (DSM) with a spatial resolution of 10 m was utilized to represent the detailed topography of the Oncheon-cheon catchment (Figure 3). Specifically, the DSM was constructed by extracting contour lines from the 1:5000 digital topographic maps provided by the National Geographic Information

Institute (NGII) of Korea, and subsequently using the triangulated irregular network (TIN) interpolation method within a Geographic Information System (GIS). This DSM was generated from digital contour maps, supplemented with river cross-section survey data and road network information, which were incorporated to realistically represent urban structures and river morphology. Cells corresponding to road areas were assigned relatively lower elevation values to more accurately simulate potential road inundation. This DSM construction methodology has been previously validated and successfully applied in urban flood modeling studies within the study domain [53]. Previous studies have demonstrated the effectiveness of such high-resolution elevation datasets for urban flood modeling in the study domain [60].

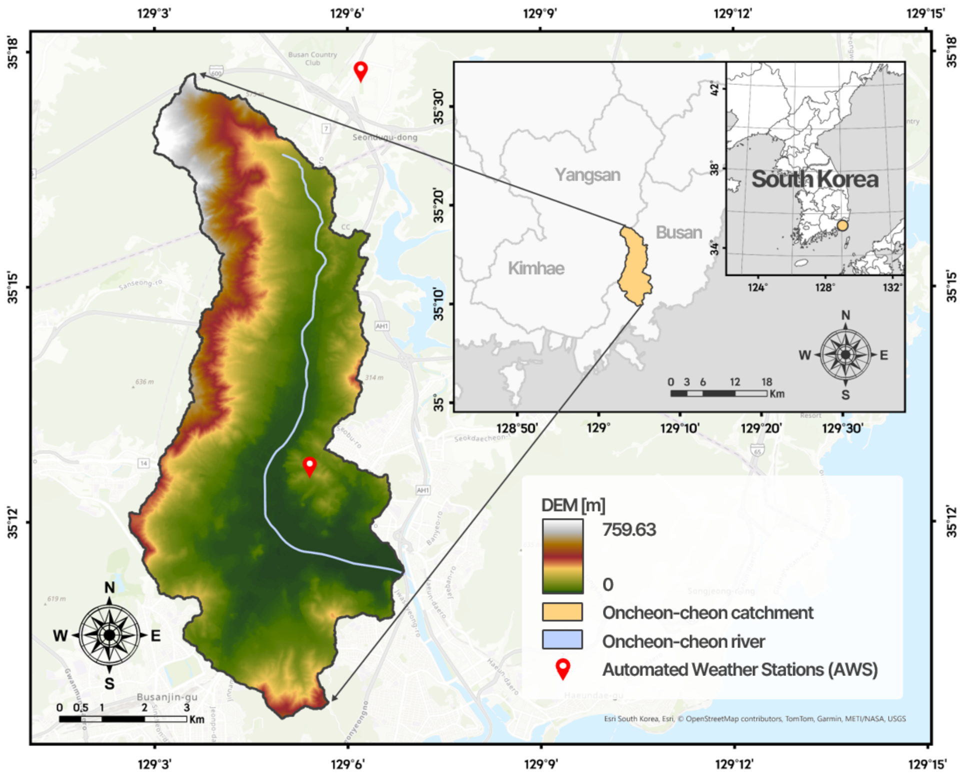

Figure 3. Study area map of the Oncheon-cheon catchment.

2.6. Experimental Setup

To generate training data for the deep learning model, synthetic precipitation scenarios were developed using probabilistic precipitation data from South Korea's National Water Resources Management Comprehensive Information System (WAMIS, http://www.wamis.go.kr/, accessed on 1 September 2024). These synthetic scenarios were classified into four distinct temporal distribution patterns: (1) early peak, (2) central peak, (3) late peak, and (4) multi-peak (double peak), each constructed at 1 h intervals to match the duration of real rainfall events for validation (Figure 4a). The synthetic rainfall patterns covered a wide range of intensities, from low-intensity events (no inundation) to extreme rainfall conditions, ensuring a comprehensive evaluation of the model's performance across different flooding scenarios. Specifically, the rainfall scenarios included total precipitation amounts corresponding to return periods of up to 50 years.

For training datasets, flood simulation results from the CADDIES-caflood model were saved at hourly intervals, ensuring a consistent temporal resolution for deep learning model development. The optimal temporal window for the rainfall time series was determined to be 4 h based on a manual sensitivity analysis, where different window sizes were tested to identify the most effective input duration for flood prediction. This selection means that the CNN model utilized the preceding 4 h rainfall data as input to predict flood inundation, balancing prediction accuracy and computational efficiency.

For validation, a synthetic rainfall event with a central-peak temporal distribution and a 20-year return period (total rainfall of 307.7 mm) was used to evaluate the model's ability to reconstruct flood conditions (Figure 4b). Additionally, an actual historical rainfall event from 2020 was selected to assess the model's predictive accuracy under real-world conditions (Figure 4c). Hourly rainfall measurements for this event were obtained from automatic weather stations (AWSs) operated by the Korea Meteorological Administration (KMA) in the Geumjeong and Dongnae districts, accessible through KMA's Open Portal. To obtain catchment-averaged precipitation, the Thiessen polygon method was applied to spatially average the hourly rainfall data from these two stations. The resulting Thiessen weights were 0.234 for the Geumjeong station and 0.766 for the Dongnae station. The locations of both AWS stations are indicated in Figure 3, providing spatial context. This event occurred from 14:00 on 23 July 2020 to 06:00 on 24 July 2020 producing a total rainfall of 174.2 mm and a peak hourly intensity of 58.8 mm.

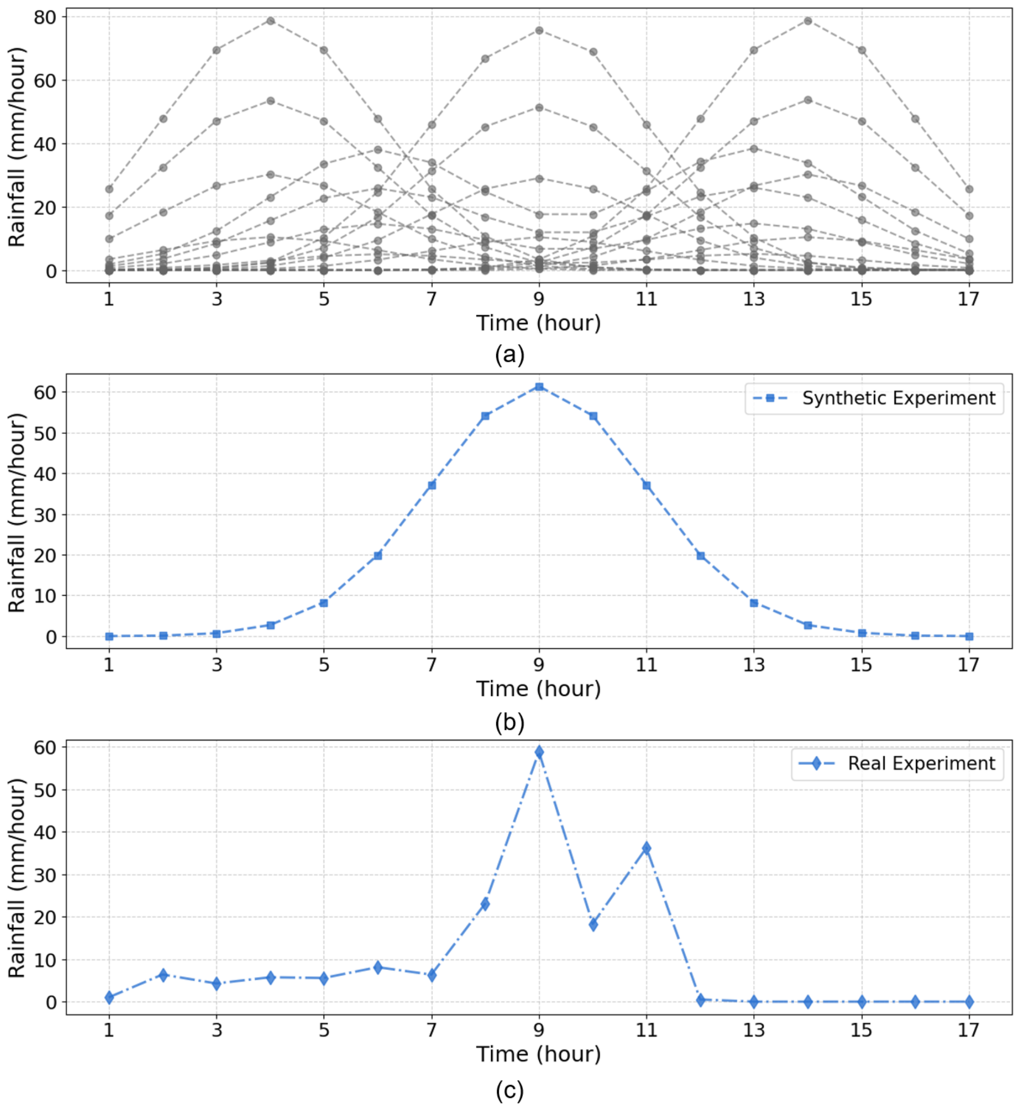

Figure 4. Rainfall time series used for model development and validation: (**a**) synthetic training event (gray), (**b**) synthetic validation event with a 20-year return period (blue), and (**c**) real validation event from 2020 (blue).

3. Results

This section presents the performance evaluation of the CNN-based flood prediction model by comparing its results with the physics-based CADDIES-caflood model. The analysis includes the spatiotemporal evolution of inundation depths, binary classification assessments, flooded area comparisons, and quantitative performance metrics under both synthetic and real flooding experiments. Additionally, the computational efficiency of the CNN model is assessed, highlighting its potential for near real-time flood forecasting.

3.1. Comparison of Spatiotemporal Evolution Between Physics-Based and Deep Learning Models

Figure 5 compares the spatiotemporal evolution of inundation depths simulated by the physics-based CADDIES-caflood model and the deep learning-based CNN model under a synthetic rainfall scenario. In this figure, buildings are overlaid solely for visualization purposes and were not incorporated into the DSM as physical features. The observed flow discontinuities and localized ponding primarily result from terrain characteristics represented in the DSM, where roads are modeled with slightly lower elevations compared with their surroundings. These topographic depressions naturally lead to water accumulation, resulting in disconnected flow paths and localized ponding. Focusing on the simulation results, overall, both models exhibit strong agreement in predicting the extent and distribution of flooding over time. At 07:00, minimal inundation is observed, with water beginning to accumulate in low-lying areas. By 10:00, flooding expands significantly along major drainage pathways and urban depressions, with both models capturing similar spatial patterns of inundation. At 13:00, slightly over the peak flooding stage, the CNN model closely follows the CADDIES-caflood results, capturing widespread inundation along the river and adjacent urban areas. The deepest floodwaters are concentrated in similar locations, particularly near the main channels and low-lying road networks. At 16:00, as water levels begin to recede, both models depict a gradual reduction in flood extent, with flooded areas contracting in a comparable manner. While the CNN model accurately represents most flood-prone areas, some discrepancies are observed in specific locations where CADDIES-caflood predicts deeper inundation, particularly in narrow streets and intersections. In the enlarged region, these differences are more noticeable at peak flooding (13:00) and during recession (16:00), where small-scale drainage complexities may not be fully captured by the CNN model. Despite these localized variations, the CNN model effectively replicates the overall flood dynamics and spatial patterns of inundation.

Figure 6 presents a spatial evaluation of CNN flood predictions compared with the physics-based CADDIES-caflood model using binary classification metrics: hits (blue), false alarms (green), and misses (red) for both the synthetic (a) and real (b) experiments. The results indicate that the CNN successfully reproduces the overall flood extent, with a high proportion of hits, demonstrating strong agreement with CADDIES-caflood. However, some differences in prediction accuracy are observed, particularly in areas with complex drainage characteristics.

In the synthetic experiment (Figure 6a), CNN predictions show relatively larger false alarms, particularly along road networks and urban depressions, suggesting slight overestimation of flooding in some areas. Misses are also present in certain flood-prone zones, indicating slight underprediction of flood extents, particularly at peak inundation. In contrast, in the real experiment (Figure 6b), CNN predictions show a notable reduction in misses, implying improved accuracy in capturing actual flood extents. However, false alarms increase, indicating that the CNN slightly overpredicts flood-prone areas under real rainfall conditions. This trade-off suggests that the CNN generalizes well to real-world events but exhibits increased sensitivity to flooding in urban environments. Despite these variations, the CNN model effectively captures the major flood patterns in both experiments, reinforcing its capability to reproduce large-scale flood dynamics while highlighting areas for further refinement in predicting localized flood variations.

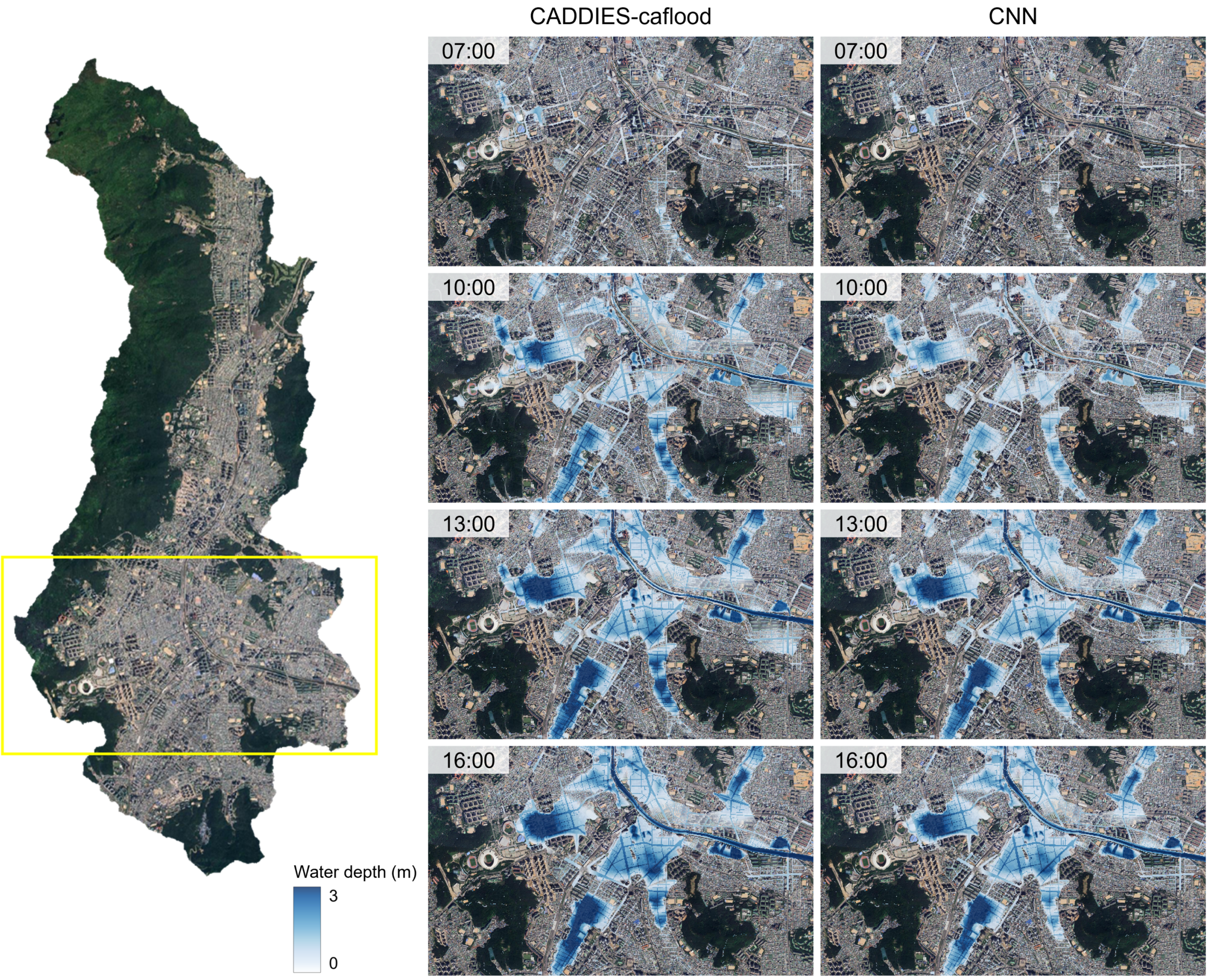

Figure 5. Comparison of spatiotemporal inundation depth evolution between CADDIES-caflood and the CNN under the synthetic rainfall scenario.

Figure 7 presents the temporal evolution of flooded areas estimated from the simulation results shown in Figure 5, comparing CADDIES-caflood and the CNN in both synthetic (a) and real (b) experiments. The flooded area is calculated based on the inundation extent at each time step, providing insight into how well the CNN model replicates the flood progression predicted by the physics-based model. The comparison highlights similarities in flood growth and peak inundation, as well as differences in the timing and extent of flood recession.

In the synthetic experiment (Figure 7a), the CNN closely follows the flood extent evolution predicted by CADDIES-caflood, with both models showing a steady increase in flooded area up to the peak at 10 h, followed by a gradual decline. Minor differences appear in the later stages, where the CNN slightly overestimates flood persistence. The agreement between the two models suggests that the CNN effectively captures the overall flood dynamics under controlled synthetic conditions.

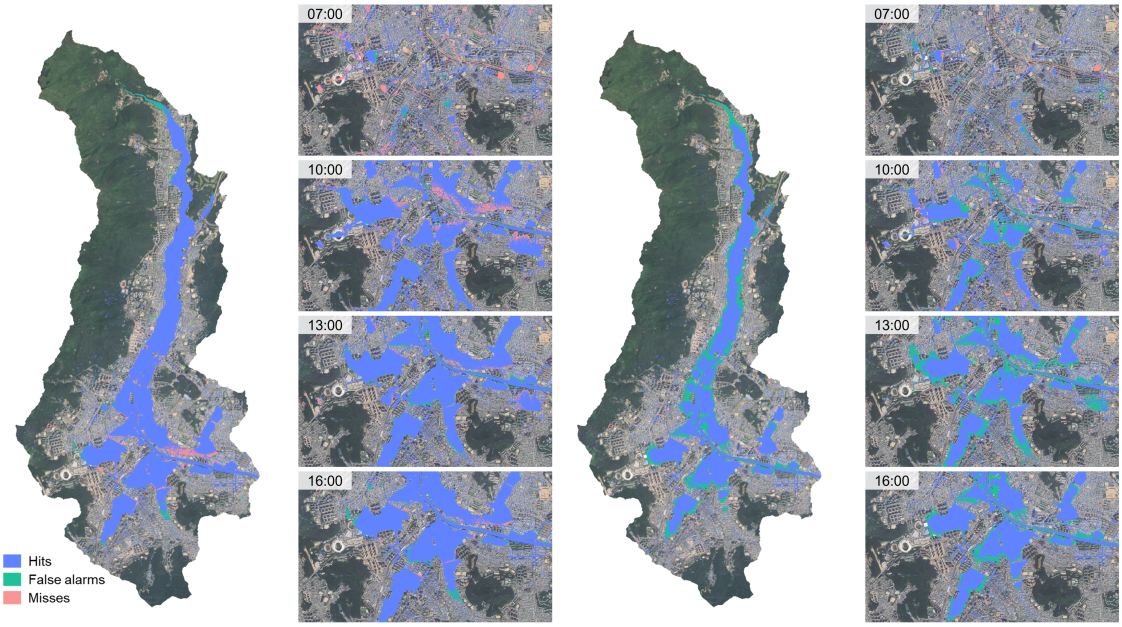

(a) Synthetic experiment

(b) Real experiment

Figure 6. Spatiotemporal evolution of binary classification metrics for the CNN compared with CADDIES-caflood in both synthetic and real experiments.

In the real experiment (Figure 7b), the CNN exhibits larger deviations, particularly in the early and late stages of flooding. The model predicts a greater flooded area in the initial phase (before 8 h) compared with CADDIES-caflood, likely due to its tendency to generalize flood expansion patterns, leading to overestimation in areas constrained by urban drainage capacity. Additionally, the CNN overpredicts peak inundation (10–14 h) and maintains a higher flooded area during the recession phase, indicating that it slower in capturing flood drainage dynamics. These trends align with Figure 5, where the CNN predicts more extensive flooding along road networks and low-lying urban zones. The overestimation observed here is also reflected in Figure 6, where the CNN shows larger false alarms in real conditions, contributing to the larger predicted flood extent. Despite these discrepancies, the CNN successfully captures the overall flood evolution trends, demonstrating its potential for flood forecasting while indicating areas for further improvement in real-world urban flood dissipation modeling.

Figure 8 illustrates the temporal evolution of CNN flood prediction performance using the CSI, HR, FAR, and Miss Rate, demonstrating how prediction accuracy changes throughout the flood event. The results indicate that the HR and CSI increase over time, while the FAR and Miss Rate decrease, suggesting that CNN predictions improve as the flood progresses. In the synthetic experiment (Figure 8a), the CSI and HR stabilize above 0.8 after 08:00, showing strong agreement with CADDIES-caflood. The FAR and Miss Rate decline consistently, indicating that the CNN initially overpredicts certain areas but corrects itself as the event unfolds. In the real experiment (Figure 8b), the CNN maintains a high HR, but the CSI exhibits slight fluctuations, ranging between 0.7 and 0.8 after 08:00. A brief decline in the HR and CSI around 09:00–10:00, alongside a temporary rise in the Miss Rate, suggests that the CNN has minor difficulties capturing flood evolution during this period. Additionally, while misses decrease in the real experiment compared with the synthetic case, the FAR is noticeably higher, consistent with Figure 6, where the CNN predicts flooding in additional areas under real conditions.

Figure 9 illustrates the temporal variation in CNN flood depth prediction accuracy using RMSE, MAE, and R^2 metrics for both the synthetic (a) and real (b) experiments. In both scenarios, R^2 increases rapidly as the flood progresses, rising from approximately 0.2 at 05:00 to above 0.8 by 08:00–10:00. The initially low R^2 values correspond to early stages with minimal flooding, where limited inundation extent reduces the effectiveness of statistical correlation. As flooding expands and affects a broader area, the CNN model demonstrates improved agreement with CADDIES-caflood, maintaining high R^2 values throughout the main flood period, with only a brief dip around 14:00 in the real experiment that quickly recovers.

RMSE values rise gradually during peak inundation phases, reflecting the increasing complexity of flood dynamics and spatial heterogeneity. In contrast, MAE remains consistently low (generally below 0.06 m) across both experiments, indicating that most depth predictions fall within a narrow error range. Both RMSE and MAE exhibit a temporary increase during peak flooding hours (approximately 10:00–14:00), which corresponds to periods of more intense and spatially complex inundation. This reflects the challenge of accurately capturing highly dynamic flood depths in certain localized areas. However, the overall error levels remain low, and the majority of predictions maintain high accuracy throughout the event.

These trends are in line with the classification-based findings presented in Figure 8, and further highlight that, despite localized discrepancies, the CNN effectively captures both the spatial distribution and temporal evolution of urban flooding. The model delivers robust performance under synthetic conditions and maintains acceptable predictive accuracy under real-world complexity, reinforcing its applicability for rapid urban flood forecasting.

Table 2 quantifies these trends by providing numerical values of the performance metrics shown in Figure 8. The table confirms that the CNN performs well in both experiments but with notable differences. In the synthetic experiment, the CNN achieves an average CSI of 0.79 and an HR of 0.85, indicating strong agreement with CADDIES-caflood. The FAR remains low at 0.11, and the Miss Rate averages 0.15, demonstrating effective flood detection with minimal false predictions. In the real experiment, the CNN maintains a high HR of 0.93, but the CSI is slightly lower at 0.73, reflecting a slight decrease in prediction accuracy. The FAR increases to 0.22, indicating a greater tendency to overpredict flood-prone areas, while the Miss Rate improves to 0.07, confirming reduced underprediction. The average RMSE is 0.15 m in the synthetic experiment and 0.17 m in the real experiment, with peak deviations occurring at 12:00–14:00 in real conditions, aligning with the overestimated flooded areas observed in Figure 7b. These findings highlight the CNN's capability to generalize flood dynamics effectively while revealing the need for refinements to improve localized accuracy in real-world urban flood modeling.

Table 2. Performance metrics in synthetic and real experiments.

	Synthetic Experiment					Real Experiment				
Time (h)	**HR**	**FAR**	**CSI**	**Misses**	**RMSE (m)**	**HR**	**FAR**	**CSI**	**Misses**	**RMSE (m)**
06:00	0.78	0.31	0.57	0.22	0.10	0.96	0.32	0.66	0.04	0.11
08:00	0.86	0.04	0.84	0.14	0.12	0.82	0.06	0.77	0.18	0.11
10:00	0.90	0.04	0.87	0.10	0.22	0.95	0.17	0.80	0.05	0.13
12:00	0.96	0.06	0.90	0.04	0.12	0.95	0.22	0.75	0.05	0.21
14:00	0.97	0.06	0.91	0.03	0.15	0.99	0.28	0.72	0.01	0.34
16:00	0.98	0.04	0.94	0.02	0.15	0.98	0.21	0.78	0.02	0.13
Average	0.85	0.11	0.79	0.15	0.15	0.93	0.22	0.73	0.07	0.17

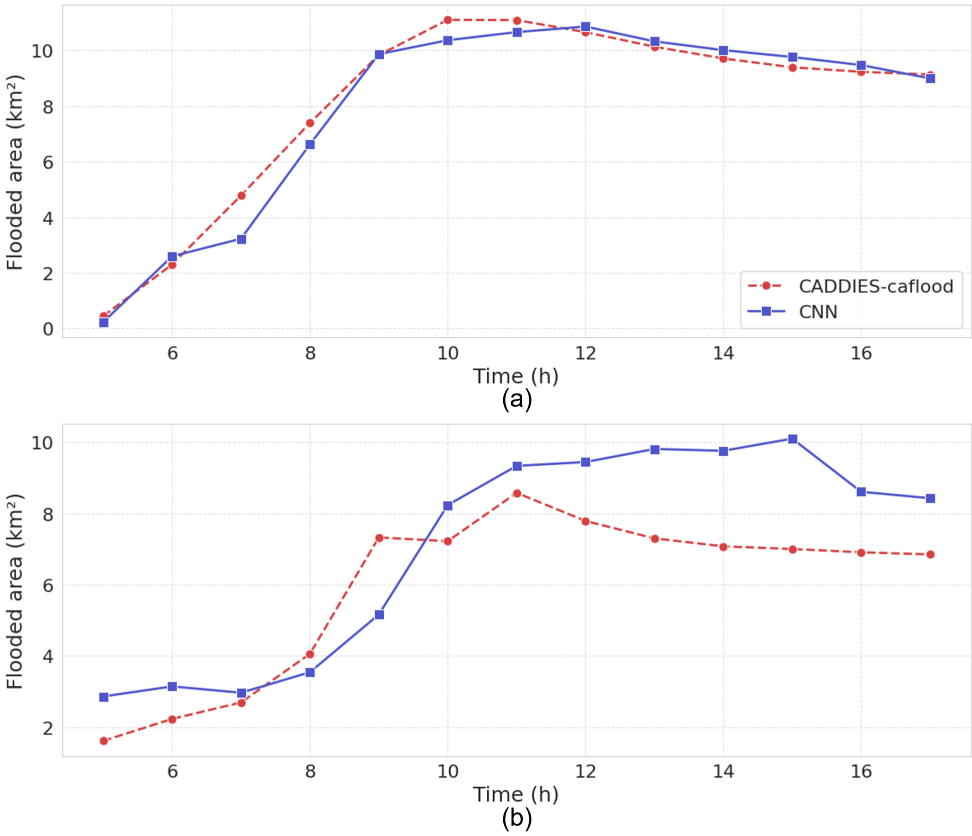

Figure 7. Comparison of flooded areas in (**a**) synthetic and (**b**) real experiments.

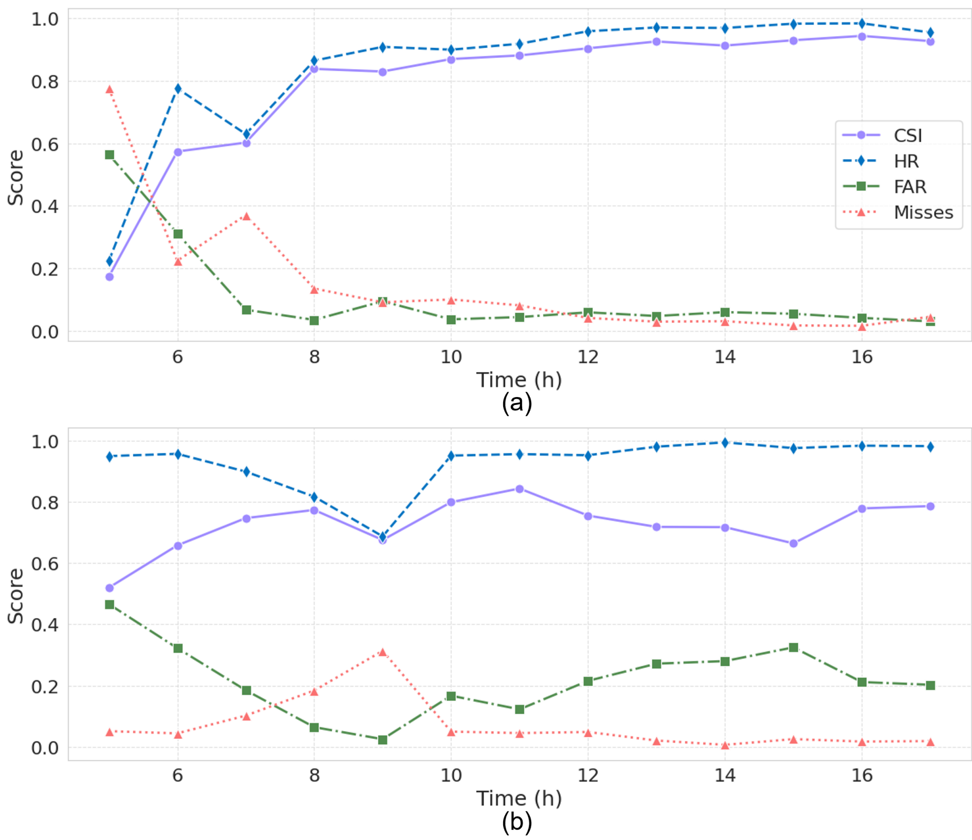

Figure 8. Comparison of binary classification measures in (**a**) synthetic and (**b**) real experiments.

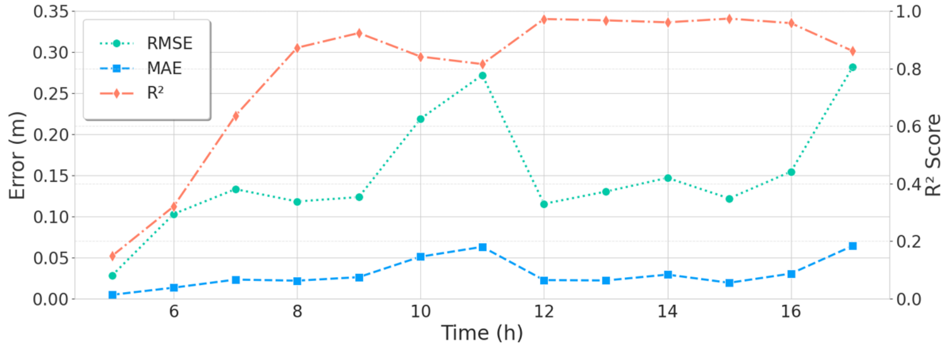

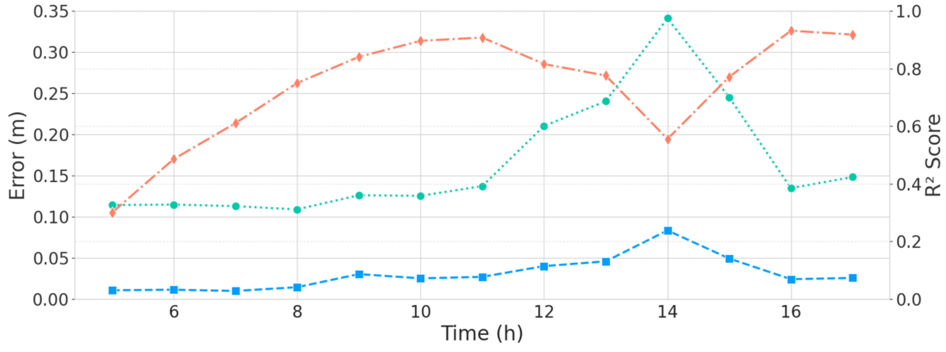

Figure 9. Comparison of performance assessment results in (**a**) synthetic and (**b**) real experiments.

3.2. Computational Efficiency

The computational efficiencies of the CNN-based surrogate model and the physics-based CADDIES-caflood model were compared using the historical event in the real experiment (17 h rainfall event from 2020, Table 3). The CADDIES-caflood model was executed on a personal computer equipped with an Intel I7-1260p CPU, 32GB RAM, and an Intel Iris Xe Graphics GPU (Intel Corp., Santa Clara, CA, USA). In contrast, the CNN model was trained and executed on Google Colab Pro Plus (Google LLC, Mountain View, CA, USA), utilizing an NVIDIA A100 GPU (NVIDIA Corp., Santa Clara, CA, USA).

For the CADDIES-caflood model, the OpenMP version, which leverages multi-core parallel computing, required approximately 121.7 s to generate the inundation maps for a single rainfall event when executed on 12 CPU cores. In contrast, the sequential computing approach using a single core took approximately 600 s. For the CNN model, training on synthetic inundation scenarios generated from probabilistic rainfall data took approximately 40 s. Once trained, the CNN model required only 7 s to predict the inundation maps for the real rainfall event, significantly reducing computation time.

To ensure a robust and fair comparison, all simulation times were estimated by averaging computation times from 10 repeated runs, reducing the impact of variability in system performance. The CNN model significantly improved computational efficiency, achieving a 98.8% reduction in computation time compared with the sequential execution of CADDIES-caflood (82.2× speedup) and a 93.9% reduction compared with the parallel execution (16.4× speedup). These results confirm the CNN model's computational advantage, making it highly suitable for near real-time flood prediction applications.

Since the CADDIES-caflood model is already more computationally efficient than conventional physics-based models, the proposed deep learning-based surrogate model further enhances computational efficiency. Our CNN-based model can generate high-resolution inundation maps in less than 10 s (approximately 7 s on average), compared with the several minutes or even hours typically required by traditional hydrodynamic models. This significant reduction in computation time effectively addresses the limitations historically associated with real-time flood forecasting. Consequently, rapid scenario analysis and timely decision support become feasible during flood events, highlighting the proposed approach as a promising tool for operational urban flood forecasting, particularly where immediate response is critical.

Table 3. Comparison of simulation time for 17 h real experiment.

Model	CADDIES-Caflood (Sequential)	CADDIES-Caflood (OpenMP)	CNN
Simulation time (s)	608.53	121.70	7.40

4. Conclusions

This study developed a deep learning-based urban flood prediction model that effectively replicates the spatiotemporal evolution of pluvial flooding simulated by physics-based hydrodynamic models. By training a CNN on synthetic precipitation scenarios and flood simulations from the CADDIES-caflood model, the study demonstrated that deep learning can serve as a computationally efficient surrogate for conventional urban flood modeling approaches.

The CNN model exhibited strong predictive performance in both synthetic and real flooding conditions, achieving high HR and CSI values. While the HR (0.85) and CSI (0.79) were higher in the synthetic experiment, the real experiment maintained a strong HR (0.93) but a slightly lower CSI (0.73), with an increased FAR, indicating a tendency to overpredict flooding, particularly along urban road networks.

A major advantage of the CNN model is its computational efficiency. In the real experiment, the CNN generated inundation maps in just 7 s, achieving a speedup 16.4 times the parallel version and 82.2 times the sequential version of the CADDIES-caflood model. These findings highlight the CNN's feasibility for near real-time urban flood prediction, making it a promising tool for operational forecasting.

Despite its strong performance, the CNN model exhibited limitations in accurately capturing localized hydrodynamic interactions, particularly under real precipitation conditions. The overprediction of flood extents suggests that further improvements are needed to better account for drainage infrastructure, urban surface roughness, and sub-grid-scale hydrodynamic features.

Further improvements could include expanding the training dataset to encompass a broader range of real rainfall events and incorporating critical hydrological variables, such as drainage infrastructure capacity and soil infiltration rates, to enhance predictive accuracy and reduce false alarms. Additionally, the fidelity of the physics-based simulations underlying our CNN model can be improved through more comprehensive environmental monitoring, including denser ground-based observation networks and high-resolution topographic and land-use data. Complementary approaches, such as citizen science initiatives, could also provide valuable flood-related observations with enhanced temporal and spatial resolution, particularly in areas lacking traditional monitoring infrastructure.

While deep learning models like CNNs offer powerful predictive capabilities, future work should also explore explainable AI techniques to improve model transparency and interpretability. Additionally, successful deployment in practice requires close collaboration with stakeholders. Developing intuitive and accessible visualization tools, and actively engaging municipal authorities, emergency management teams, and urban planners will help ensure that flood predictions are effectively translated into actionable insights for decision-making in urban flood management.

Future research should further incorporate additional physical constraints into the model training process by leveraging hybrid physics-guided deep learning methods to enhance model transferability and physical realism. A promising direction is the integration of Physics-Informed Neural Networks (PINNs), which embed conservation laws directly within neural network architectures. For example, embedding the Shallow Water Equations into the PINN loss function serves as a regularization mechanism, guiding the model to learn physically plausible solutions, even in sparse-data or unseen scenarios [61–63]. Such integration could significantly improve predictive accuracy for extreme events and strengthen the physical consistency of flood predictions. However, addressing implementation challenges in complex urban settings remains an important consideration for future studies.

Overall, this study demonstrates the potential of deep learning as a fast and reliable alternative to conventional physics-based urban flood modeling. By combining deep learning with physics-based simulations, the proposed approach offers a cost-effective, high-resolution, and computationally efficient method for urban flood forecasting, paving the way for more adaptive and scalable flood risk management strategies.

Author Contributions: Conceptualization, H.W. and S.J.N.; methodology, H.W. and S.J.N.; software, H.W., H.C., M.K. and S.J.N.; analysis, H.W., H.C., M.K. and S.J.N.; writing—original draft preparation, H.W.; writing—review and editing, H.W., H.C., M.K. and S.J.N.; supervision, S.J.N. All authors have read and agreed to the published version of the manuscript.

Funding: This work was supported by a Korea Environment Industry & Technology Institute (KEITI) grant, funded by the Korea Ministry of Environment (MOE) (RS-2023-00218973), Korea Environmental Industry & Technology Institute (KEITI) through the R&D Program for Innovative Flood Protection Technologies against Climate Crisis, funded by the Korea Ministry of Environment (MOE) (2022003470001), and the Technology Innovation Program (RS202400398858, development of AI-based urban flood damage risk prediction and evaluation technology for practical use), funded by the Ministry of the Interior and Safety (MOIS, Korea).

Data Availability Statement: The data used in this study are available upon request.

Conflicts of Interest: The authors declare no conflicts of interest.

References

1. Woo, H.; Choi, H.; Kim, M.; Noh, S.J. Estimating urban inundation using physics-informed deep learning: A case study of the Oncheon-cheon catchment. *J. Korea Water Resour. Assoc.* **2024**, *57*, 989–1001. [CrossRef]
2. Cao, W.; Zhou, Y.; Güneralp, B.; Li, X.; Zhao, K.; Zhang, H. Increasing global urban exposure to flooding: An analysis of long-term annual dynamics. *Sci. Total Environ.* **2022**, *817*, 153012. [CrossRef]
3. Tang, Z.; Wang, P.; Li, Y.; Sheng, Y.; Wang, B.; Popovych, N.; Hu, T. Contributions of climate change and urbanization to urban flood hazard changes in China's 293 major cities since 1980. *J. Environ. Manag.* **2024**, *353*, 120113. [CrossRef]
4. Azizi, K.; Diko, S.K.; Saija, L.; Zamani, M.G.; Meier, C.I. Integrated community-based approaches to urban pluvial flooding research, trends and future directions: A review. *Urban Clim.* **2022**, *44*, 101237. [CrossRef]
5. Yang, F.; Ding, W.; Zhao, J.; Song, L.; Yang, D.; Li, X. Rapid urban flood inundation forecasting using a physics-informed deep learning approach. *J. Hydrol.* **2024**, *643*, 131998. [CrossRef]
6. Jiang, C.; Kang, Y.; Qu, K.; Long, Y.; Ma, Y.; Yan, S. Towards a high-resolution modelling scheme for local-scale urban flood risk assessment based on digital aerial photogrammetry. *Eng. Appl. Comput. Fluid Mech.* **2023**, *17*, 2240392. [CrossRef]
7. Liu, W.; Feng, Q.; Engel, B.A.; Yu, T.; Zhang, X.; Qian, Y. A probabilistic assessment of urban flood risk and impacts of future climate change. *J. Hydrol.* **2023**, *618*, 129267. [CrossRef]
8. Qi, W.; Ma, C.; Hongshi, X.; Zifan, C.; Zhao, K.; Han, H. A review on applications of urban flood models in flood mitigation strategies. *Nat. Hazards* **2021**, *108*, 31–62. [CrossRef]
9. Sanders, B.F. Hydrodynamic Modeling of Urban Flood Flows and Disaster Risk Reduction. In *Oxford Research Encyclopedia of Natural Hazard Science*; Oxford University Press: Oxford, UK, 2017. [CrossRef]

10. Lee, S.; Kim, B.; Choi, H.; Noh, S.J. A review on urban inundation modeling research in South Korea: 2001–2022. *J. Korea Water Resour. Assoc.* **2022**, *55*, 707–721. [CrossRef]
11. Wing, O.E.J.; Bates, P.D.; Sampson, C.C.; Smith, A.M.; Johnson, K.A.; Erickson, T.A. Validation of a 30 m resolution flood hazard model of the conterminous United States. *Water Resour. Res.* **2017**, *53*, 7968–7986. [CrossRef]
12. Jiang, L.; Chen, Y.; Wang, H. Urban flood simulation based on the SWMM model. *Proc. IAHS* **2015**, *368*, 186–191. [CrossRef]
13. Neal, J.; Dunne, T.; Sampson, C.; Smith, A.; Bates, P. Optimisation of the two-dimensional hydraulic model LISFOOD-FP for CPU architecture. *Environ. Model. Softw.* **2018**, *107*, 148–157. [CrossRef]
14. Bulti, D.T.; Abebe, B.G. A review of flood modeling methods for urban pluvial flood application. *Model. Earth Syst. Environ.* **2020**, *6*, 1293–1302. [CrossRef]
15. Guo, K.; Guan, M.; Yu, D. Urban surface water flood modelling—A comprehensive review of current models and future challenges. *Hydrol. Earth Syst. Sci.* **2021**, *25*, 2843–2860. [CrossRef]
16. Henonin, J.; Russo, B.; Mark, O.; Gourbesville, P. Real-time urban flood forecasting and modelling—A state of the art. *J. Hydroinformatics* **2013**, *15*, 717–736. [CrossRef]
17. Kim, H.I.; Han, K.Y.; Lee, J.Y. Prediction of Urban Flood Extent by LSTM Model and Logistic Regression. *J. Korean Soc. Civ. Eng.* **2020**, *40*, 273–283. [CrossRef]
18. Guo, K.; Guan, M.; Yan, H.; Xia, X. A spatially distributed hydrodynamic model framework for urban flood hydrological and hydraulic processes involving drainage flow quantification. *J. Hydrol.* **2023**, *625*, 130135. [CrossRef]
19. Hasan, H.H.; Mohd Razali, S.F.; Ahmad Zaki, A.Z.I.; Mohamad Hamzah, F. Integrated Hydrological-Hydraulic Model for Flood Simulation in Tropical Urban Catchment. *Sustainability* **2019**, *11*, 6700. [CrossRef]
20. Abdessamed, D.; Abderrazak, B. Coupling HEC-RAS and HEC-HMS in rainfall–runoff modeling and evaluating floodplain inundation maps in arid environments: Case study of Ain Sefra city, Ksour Mountain. SW of Algeria. *Environ. Earth Sci.* **2019**, *78*, 586. [CrossRef]
21. Natarajan, S.; Radhakrishnan, N. An Integrated Hydrologic and Hydraulic Flood Modeling Study for a Medium-Sized Ungauged Urban Catchment Area: A Case Study of Tiruchirappalli City Using HEC-HMS and HEC-RAS. *J. Inst. Eng. (India) Ser. A* **2020**, *101*, 381–398. [CrossRef]
22. Peker, İ.B.; Gülbaz, S.; Demir, V.; Orhan, O.; Beden, N. Integration of HEC-RAS and HEC-HMS with GIS in Flood Modeling and Flood Hazard Mapping. *Sustainability* **2024**, *16*, 1226. [CrossRef]
23. Noh, S.J.; Lee, J.H.; Lee, S.; Kawaike, K.; Seo, D.J. Hyper-resolution 1D-2D urban flood modelling using LiDAR data and hybrid parallelization. *Environ. Model. Softw.* **2018**, *103*, 131–145. [CrossRef]
24. Morales-Hernández, M.; Sharif, M.B.; Kalyanapu, A.; Ghafoor, S.K.; Dullo, T.T.; Gangrade, S.; Kao, S.C.; Norman, M.R.; Evans, K.J. TRITON: A Multi-GPU open source 2D hydrodynamic flood model. *Environ. Model. Softw.* **2021**, *141*, 105034. [CrossRef]
25. Luan, G.; Hou, J.; Wang, T.; Li, D.; Zhou, Q.; Liu, L.; Duan, C. A 1D-2D dynamic bidirectional coupling model for high-resolution simulation of urban water environments based on GPU acceleration techniques. *J. Clean. Prod.* **2023**, *428*, 139494. [CrossRef]
26. Dottori, F.; Todini, E. Developments of a flood inundation model based on the cellular automata approach: Testing different methods to improve model performance. *Phys. Chem. Earth Parts A/B/C* **2011**, *36*, 266–280. [CrossRef]
27. Ghimire, B.; Chen, A.S.; Guidolin, M.; Keedwell, E.C.; Djordjević, S.; Savić, D.A. Formulation of a fast 2D urban pluvial flood model using a cellular automata approach. *J. Hydroinformatics* **2012**, *15*, 676–686. [CrossRef]
28. Guidolin, M.; Chen, A.S.; Ghimire, B.; Keedwell, E.C.; Djordjević, S.; Savić, D.A. A weighted cellular automata 2D inundation model for rapid flood analysis. *Environ. Model. Softw.* **2016**, *84*, 378–394. [CrossRef]
29. Cea, L.; Sañudo, E.; Montalvo, C.; Farfán, J.; Puertas, J.; Tamagnone, P. Recent advances and future challenges in urban pluvial flood modelling. *Urban Water J.* **2025**, *22*, 149–173. [CrossRef]
30. Assumpção, T.H.; Popescu, I.; Jonoski, A.; Solomatine, D.P. Citizen observations contributing to flood modelling: Opportunities and challenges. *Hydrol. Earth Syst. Sci.* **2018**, *22*, 1473–1489. [CrossRef]
31. Guo, K.; Guan, M.; Yan, H. Utilising social media data to evaluate urban flood impact in data scarce cities. *Int. J. Disaster Risk Reduct.* **2023**, *93*, 103780. [CrossRef]
32. Alemu, A.N.; Haile, A.T.; Carr, A.B.; Trigg, M.A.; Mengistie, G.K.; Walsh, C.L. Filling data gaps using citizen science for flood modeling in urbanized catchment of Akaki. *Nat. Hazards Res.* **2023**, *3*, 395–407. [CrossRef]
33. Yan, Z.; Guo, X.; Zhao, Z.; Tang, L. Achieving fine-grained urban flood perception and spatio-temporal evolution analysis based on social media. *Sustain. Cities Soc.* **2024**, *101*, 105077. [CrossRef]
34. Zhou, Y.; Wu, W.; Nathan, R.; Wang, Q.J. A rapid flood inundation modelling framework using deep learning with spatial reduction and reconstruction. *Environ. Model. Softw.* **2021**, *143*, 105112. [CrossRef]
35. Kabir, S.; Patidar, S.; Xia, X.; Liang, Q.; Neal, J.; Pender, G. A deep convolutional neural network model for rapid prediction of fluvial flood inundation. *J. Hydrol.* **2020**, *590*, 125481. [CrossRef]
36. Hosseiny, H. A deep learning model for predicting river flood depth and extent. *Environ. Model. Softw.* **2021**, *145*, 105186. [CrossRef]

37. Zhou, Q.; Teng, S.; Situ, Z.; Liao, X.; Feng, J.; Chen, G.; Zhang, J.; Lu, Z. A deep-learning-technique-based data-driven model for accurate and rapid flood predictions in temporal and spatial dimensions. *Hydrol. Earth Syst. Sci.* **2023**, *27*, 1791–1808. [CrossRef]
38. Nearing, G.; Cohen, D.; Dube, V.; Gauch, M.; Gilon, O.; Harrigan, S.; Hassidim, A.; Klotz, D.; Kratzert, F.; Metzger, A.; et al. Global prediction of extreme floods in ungauged watersheds. *Nature* **2024**, *627*, 559–563. [CrossRef]
39. Chen, J.; Li, Y.; Zhang, S. Fast Prediction of Urban Flooding Water Depth Based on CNN–LSTM. *Water* **2023**, *15*, 1397. [CrossRef]
40. Xu, L.; Gao, L. A hybrid surrogate model for real-time coastal urban flood prediction: An application to Macao. *J. Hydrol.* **2024**, *642*, 131863. [CrossRef]
41. Wang, Y.; Fang, Z.; Hong, H.; Peng, L. Flood susceptibility mapping using convolutional neural network frameworks. *J. Hydrol.* **2020**, *582*, 124482. [CrossRef]
42. Seleem, O.; Ayzel, G.; Bronstert, A.; Heistermann, M. Transferability of data-driven models to predict urban pluvial flood water depth in Berlin, Germany. *Nat. Hazards Earth Syst. Sci.* **2023**, *23*, 809–822. [CrossRef]
43. Pal, S.; Saha, A.; Gogoi, P.; Saha, S. An Ensemble of J48 Decision Tree with AdaBoost and Bagging for Flood Susceptibility Mapping in the Sundarbans of West Bengal, India. In *Geomorphic Risk Reduction Using Geospatial Methods and Tools*; Springer: Singapore, 2024; pp. 117–133. [CrossRef]
44. Bukhari, S.A.S.; Shafi, I.; Ahmad, J.; Butt, H.T.; Khurshaid, T.; Ashraf, I. Enhancing flood monitoring and prevention using machine learning and IoT integration. *Nat. Hazards* **2025**, *121*, 4837–4864. [CrossRef]
45. Bukhari, S.A.S.; Shafi, I.; Ahmad, J.; Villar, S.G.; Villena, E.G.; Khurshaid, T.; Ashraf, I. Review of flood monitoring and prevention approaches: A data analytic perspective. *Nat. Hazards* **2024**. [CrossRef]
46. Löwe, R.; Böhm, J.; Jensen, D.G.; Leandro, J.; Rasmussen, S.H. U-FLOOD—Topographic deep learning for predicting urban pluvial flood water depth. *J. Hydrol.* **2021**, *603*, 126898. [CrossRef]
47. Hofmann, J.; Schüttrumpf, H. floodGAN: Using Deep Adversarial Learning to Predict Pluvial Flooding in Real Time. *Water* **2021**, *13*, 2255. [CrossRef]
48. Burrichter, B.; Hofmann, J.; Koltermann da Silva, J.; Niemann, A.; Quirmbach, M. A Spatiotemporal Deep Learning Approach for Urban Pluvial Flood Forecasting with Multi-Source Data. *Water* **2023**, *15*, 1760. [CrossRef]
49. Kumar, V.; Azamathulla, H.M.; Sharma, K.V.; Mehta, D.J.; Maharaj, K.T. The State of the Art in Deep Learning Applications, Challenges, and Future Prospects: A Comprehensive Review of Flood Forecasting and Management. *Sustainability* **2023**, *15*, 10543. [CrossRef]
50. Karniadakis, G.E.; Kevrekidis, I.G.; Lu, L.; Perdikaris, P.; Wang, S.; Yang, L. Physics-informed machine learning. *Nat. Rev. Phys.* **2021**, *3*, 422–440. [CrossRef]
51. Bhattarai, Y.; Bista, S.; Talchabhadel, R.; Duwal, S.; Sharma, S. Rapid prediction of urban flooding at street-scale using physics-informed machine learning-based surrogate modeling. *Total Environ. Adv.* **2024**, *12*, 200116. [CrossRef]
52. Guglielmo, G.; Montessori, A.; Tucny, J.M.; La Rocca, M.; Prestininzi, P. A priori physical information to aid generalization capabilities of neural networks for hydraulic modeling. *Front. Complex Syst.* **2025**, *2*, 1508091. [CrossRef]
53. Choi, H.; Lee, S.; Woo, H.; Noh, S.J. High-resolution Urban Flood Modeling using Cellular Automata-based WCA2D in the Oncheon-cheon Catchment in Busan, South Korea. *Ksce J. Civ. Environ. Eng. Res.* **2023**, *43*, 587–599. [CrossRef]
54. Gibson, M.J.; Savic, D.A.; Djordjevic, S.; Chen, A.S.; Fraser, S.; Watson, T. Accuracy and Computational Efficiency of 2D Urban Surface Flood Modelling Based on Cellular Automata. *Procedia Eng.* **2016**, *154*, 801–810. [CrossRef]
55. Cao, R.; Li, F.; Feng, P. Exploring the hydrologic response to the urban building coverage ratio by model simulation. *Theor. Appl. Climatol.* **2020**, *140*, 1005–1015. [CrossRef]
56. Lee, S.; Choi, H.; Woo, H.; Kim, M.; Lee, E.; Kim, S.; Noh, S.J. Development and application of cellular automata-based urban inundation and water cycle model CAW. *J. Korea Water Resour. Assoc.* **2024**, *57*, 165–179. [CrossRef]
57. Rasool, U.; Yin, X.; Xu, Z.; Rasool, M.A.; Hussain, M.; Siddique, J.; Hai, N.T. Quantifying pluvial flood simulation in ungauged urban area; A case study of 2022 unprecedented pluvial flood in Karachi, Pakistan. *J. Hydrol.* **2025**, *655*, 132905. [CrossRef]
58. EA. *What is the Risk of Flooding from Surface Water Map?* Environment Agency: Bristol, UK, 2019.
59. Woo, H. Estimating Urban Inundation Using Physics-Informed Deep Learning. Master's Thesis, Kumoh National Institute of Technology, Gumi, Republic of Korea, 2025.
60. Shon, T.S.; Kang, D.H.; Jang, J.K.; Shin, H.S. A study of Assessment for Internal Inundation Vulnerability in Urban Area using SWMM. *J. Korean Soc. Hazard Mitig.* **2010**, *10*, 105–117.
61. Feng, D.; Tan, Z.; He, Q. Physics-Informed Neural Networks of the Saint-Venant Equations for Downscaling a Large-Scale River Model. *Water Resour. Res.* **2023**, *59*, e2022WR033168. [CrossRef]

62. Donnelly, J.; Daneshkhah, A.; Abolfathi, S. Physics-informed neural networks as surrogate models of hydrodynamic simulators. *Sci. Total Environ.* **2024**, *912*, 168814. [CrossRef]
63. Qi, X.; de Almeida, G.A.M.; Maldonado, S. Physics-informed neural networks for solving flow problems modeled by the 2D Shallow Water Equations without labeled data. *J. Hydrol.* **2024**, *636*, 131263. [CrossRef]